Title
High-throughput Computational Study of Halide Double Perovskite Inorganic Compounds

Journal
Chemistry of Materials, 31(15)

ISSN
0897-4756

Authors
Cai, Y
Xie, W
Teng, YT
et al.

Publication Date
2019-08-13

DOI
10.1021/acs.chemmater.9b00116

Peer reviewed

High-throughput Computational Study of Halide Double Perovskite Inorganic Compounds

Yao Cai,[*,†] Wei Xie,[†] Teng Yin Ting,[‡] Harikesh Padinhare Cholakkal,[¶] Ghosh Biplab,[¶] Patrick Huck,[§] Kristin A. Persson,[§,†] Nripan Mathews,[¶,‡] Subodh G. Mhaisalkar,[¶,‡] Matthew Sherburne,[†] and Mark Asta[*,†,‖]

†*Department of Materials Science and Engineering, University of California, Berkeley, California, USA*

‡*Energy Research Institute @ NTU (ERI@N), Interdisciplinary Graduate School, Nanyang Technological University, Singapore*

¶*School of Materials Science and Engineering, Nanyang Technological University, Singapore*

§*Energy Storage and Distributed Resources Division, Lawrence Berkeley National Laboratory, Berkeley, California, USA*

‖*Materials Sciences Division, Lawrence Berkeley National Laboratory, Berkeley, California, USA*

E-mail: yaocai@berkeley.edu; mdasta@berkeley.edu

Abstract

Double perovskite halides are a class of materials with diverse chemistries that are amenable to solution-based synthesis routes, and display a range of properties for diverse potential applications. Starting from a consideration of the octahedral and tolerance factors of 2000 candidate double-perovskite compounds, we compute structural, electronic and transport properties of 1000 compounds using first-principles

calculations. The computational results have been assembled in a database that is accessible through the Materials Project online. As one potential application, double perovskites are promising candidates in the search for lead-free halide photovoltaic absorbers. We present the application of our database to aid the discovery of new double perovskite halide photovoltaic materials. Forty compounds from five categories were identified as promising solar absorber candidates and the complex chemical trends for band gap within each category are analyzed, to provide guidelines for the use of subtitutional alloying as a means of tuning the electronic structure. Other possible applications of the database are also discussed briefly.

Introduction

Double perovskite halides($A_2BB'X_6$) are a class of compounds that can incorporate diverse chemistries. The crystal structure(Figure 1(a)) is formed by corner-sharing octahedra with B or B′ atoms at the centers and X atoms at corners. B and B′ centers are ordered as second neighbors over the simple cubic cation sublattice and A atoms are in the center of eight neighboring octahedra. Due to its diverse chemistries, the family of halide double perovskites display a range of electronic properties, making them candidates for a range of applications, including photo-absorbers for solar cells, UV photodetectors, X-ray detector, and scintillators, etc. For example, thin film $Cs_2AgBiBr_6$ photovoltaic devices were demonstrated with Power Conversion Efficiency(PCE) close to 2.5% and a open circuit voltage exceeding one volt[1]; sensitive and fast UV photodetectors based on $Cs_2AgInCl_6$ single crystals[2] and low detection limit X-ray detectors based on $Cs_2AgBiBr_6$ single crystal were demonstrated[3], respectively; Cs_2LiYCl_6 can detect Gamma ray, thermal and fast neutrons simultaneously[4]. The wide interest and diverse range of potential applications of these compounds has motivated the current work, in which we have employed high-throughput computing to develop an open and searchable double perovskite halide database, which has been incorporated into Materials Project database[5].

One of the applications of double perovskite halides that has received significant attention recently is as absorber materials for solar cells[6]. Many experimental and computational works of this topic have been published since 2016. Single crystal of $Cs_2AgBiBr_6$(indirect band gap 1.95 eV) was synthesized and shown to have a long room-temperature fundamental photoluminescence(PL) lifetime of 660 ns, high defect tolerance and better heat and moisture stability compared with $(MA)PbI_3$[7]. Another work demonstrates long electron-hole diffusion length(> 100 nm) in $Cs_2AgBiBr_6$ solar cell devices with over 1% PCE[8]. The hybrid double perovskite $(MA)_2AgBiBr_6$ with a band gap of 2.02 eV was also synthesized[9]. $Cs_2AgBiCl_6$ was synthesized with an indirect band gap of 2.2[10] $\sim$ 2.77 eV[11], and Cs_2AgBiI_6 with a smaller 1.75 eV band gap was synthesized as nanocrystals via anion-exchange[12]. A similar compound $Cs_2AgSbCl_6$ with an indirect band gap(2.54 eV)[13] was also synthesized. Another double perovskite $(MA)_2KBiCl_6$ was synthesized and found to have a large indirect band gap of 3.04 eV[14]. Indirect band gaps are not ideal for photovoltaic applications, and direct band gap materials are desired[15]. Single crystal $(MA)_2TlBiBr_6$ was synthesized and found to have an direct band gap of 2.0 eV[16]. $Cs_2AgInCl_6$, a direct band gap compound with parity-forbidden band gap of 2.1 eV and absorption onset of 3.2 eV[2] was shown to be photosensitive to UV light[17], and have good moisture, light and heat stability[18].

As a means for further optimizing the properties of double perovskites for device applications, substitutional alloying or doping is expected to be a useful strategy. Band engineering with impurities in this system can dramatically alter band edge structure. Dilute alloying of Tl into both Ag and Bi sites of $Cs_2AgBiBr_6$ decreases its band gap by 0.5 eV, with long-lived carriers with micro-second lifetimes[19]. 75%In and 37.5%Sb can be alloyed into the host $Cs_2AgBiBr_6$ with In-Bi alloying increasing the band gap and Sb-Bi alloying decreasing the band gap to 1.86 eV at most[20]. Solid solutions between $Cs_2AgSbCl_6$ and $Cs_2AgInCl_6$ can be tuned to have either direct(below 40%Sb) or indirect(above 40%Sb) band gaps[13]. A DFT study indicates that $Cs_2BiAg_{1-x}Cu_xCl_6$ mixes should be amenable to synthesis with the band gap between 1.6 $\sim$ 1.9 eV[21]. Another DFT study indicates that mixed-cation

$(Cs/MA/FA)_2InBiBr_6$ halide double perovskites have optoelectronic properties comparable to $MAPbI_3$[22].

Several works have focused on the computational screening of double perovskites for photovoltaic applications. Two double perovskites $Cs_2InSbCl_6$ and $Cs_2InBiCl_6$ isoelectronic to Pb halides(ns^2np^0) were proposed as promising candidates due to their good theoretical maximum solar cell efficiencies[23,24]. Also proposed were three other double perovskites $Cs_2AgInBr_6$, $Rb_2AgInBr_6$ and $Rb_2CuInCl_6$ that have direct band gaps with close to optimal values for solar absorbers[25,26]. $Rb_2AgInCl_6$ and $Cs_2AgInCl_6$ with larger direct band gaps are another two stable compounds identified from another computational study[27]. Mixed valence $Cs_2Au_2I_6$ was shown to be a direct gap semiconductor with a 1.31 eV gap by first-principles calculations[28].

The experimental and computational works reviewed above have focused on a relatively small number($\sim$ 50) of halide double perovskite compositions, considering the very large number of possible compositions. Consequently, an expanded computational screening effort that considers a wider range of chemical combinations is worthwhile. In this work, we performed density functional theory(DFT) based high-throughput calculations considering $\sim$2000 halide double perovskites. Based on our calculations we have developed a double perovskite database, including all calculated structural information, energetics, and band gaps. We will first screen $\sim$2000 double perovskites against empirical structural factors and thermodynamic stability. Next, we employ semi-local DFT functionals(Perdew-Burke-Ernzerhof parametrization of the generalized gradient approximation, or GGA-PBE[29]) to perform electronic structure calculations on possible stable compounds to obtain a rough estimate of band gaps.

As an application of this database, we present the application of this database to aid the discovery of new photovoltaic(PV) materials and explore trends underlying the variation of electronic structure with chemical composition. 40 double perovskites from our database are identified as possible candidates as solar absorbers. For these compounds we employ

hybrid-functional (HSE06) methods with spin-orbit coupling to calculate and analyze the electronic structures in more detail. The important parameters for PV applications, such as band gaps and effective masses, are calculated. Importantly, the 40 double perovskite compounds are divided into five categories by the nature of their band edge characters. Several compounds from three of the five categories have been reported in previous experimental or computational studies (A_2AgBiX_6[7,8,10,12], A_2AgSbX_6[13], A_2AgInX_6[2,17,18,27], A_2CuInX_6[25], A_2TlBiX_6[16], A_2InBiX_6[23] and A_2InSbX_6[23], etc), and our results have confirmed these. Furthermore, we propose two new categories of compounds in this work: $A_2BB'X_6$ with B=Cu, Ag, Au, B′=Sc, Y; $A_2BB'X_6$ with B=In, Tl, B′=Al, Ga, In, Tl. Inside each category, chemical trends of band gaps are discussed, and these trends provide guidance for design of solid solutions between two double perovskites.

The results yield the following chemical trends. For all $Cs_2BB'Cl_6$ compounds with B = Cu, Ag, Au and B′=Al, Ga, In, Tl, Sc, Y, As, Sb, Bi, silver compounds always have larger band gaps than Cu and Au with the same B′ elements. This result is consistent with previously reported trends for Cs_2BBiCl_6[23]. For $Cs_2BB'Cl_6$ compounds with B = Cu, Ag, Au and B′ = Al, Ga, In, Tl, the band gap trend for B′ site is Al > In, Ga > Tl. For $Cs_2BB'Cl_6$ compounds with B = In, Tl and B′ = As, Sb, Bi, thallium compounds have larger band gaps than In compounds, which is consistent with previous reports[23]. For $Cs_2BB'Cl_6$ compounds with B = Cu, Ag, Au and B′ = As, Sb, Bi, the band gap trend for B′ is Bi > Sb > As. For $Cs_2BB'Cl_6$ compounds with B=Cu, Ag, Au and B′ = Sc, Y, band gap increases from Sc to Y. For $Cs_2BB'Cl_6$ compounds with B = In, Tl and B′ = Al, Ga, In, Tl, the larger the difference in electronegativity between B and B′ elements, the larger the band gap.

Database Details

In this section we describe the methods underlying the development of the double perovskite computational database, the results of screening based on consideration of tolerance and octa-

hedral factors to identify the chemistries considered, and an overview of the database information. The database of calculated values can be accessed through the Materials Project website(DOI: 10.17188/1476059, link: https://materialsproject.org/materials/10.17188/1476059).

Computational Methods

Calculations were carried out employing spin-polarized HSE06 and PBE-GGA based DFT methods using the Projector Augmented Wave (PAW) method[30], as implemented in the Vienna Ab initio simulation package (VASP)[31–33]. The PAW potentials used in the calculations are the same as those used in the calculations underlying the data in Materials Project[5], in order to facilitate comparisons with the results available through this database. The self-consistency iterations were performed until the energy was converged to within 1×10^{-5} eV. Structural relaxations were undertaken until the forces were converged within 0.01 $eV/\mathring{A}$ for the GGA-PBE calculations, and within 0.05 $eV/\mathring{A}$ for HSE06. The energy cutoff for the plane wave basis for all compounds was set to 520 eV. Relaxation calculations were carried out with a gamma-centered k-point mesh of 5×5×5. Based on our convergence tests, this choice of plane-wave cutoff and k-point density is found to be sufficient to provide total energies converged to within 1 meV/atom, and lattice constants within 0.01 Å.

To obtain more accurate electronic structures for select compounds, band structures and density of states were calculated by PBE with spin-orbit coupling (SOC) corrections, with conduction bands shifted to match the HSE06+SOC band gaps. Spin-orbit coupling was included using the approach available in VASP. For density of states calculations, a gamma-centered k-point mesh of 10×10×10 and the tetrahedron method with Blöchl corrections was used for k-space integration. For band structure calculations, k-points were sampling along high-symmetry lines in the Brillouin zone.

The energy above hull(i.e., the difference in energy between this compound and the compound or phase-separated combinations of compounds that have the lowest energy at the associated composition) was calculated by retrieving the total energies of all available

compounds in A-B-B′-X system from Materials Project, including common allotropes, binary and ternary compounds.

The average effective masses[34] were calculated using the BoltzTrap code[35] and the pymatgen package[34,36]. Gamma-centered 20×20×20 k-point meshes were used for GGA-PBE band structure calculations. The band structures were then used as input to the BoltzTrap code to calculate the conductivity tensor $\frac{\sigma(T,\mu)}{\tau}$, with τ the constant relaxation time, the temperature(T) is set to 300K, and μ the Fermi level. Then averaged effective masses were calculated as $\mathbf{m} = \frac{ne^2\tau}{\sigma}$. As mentioned by Hautier et al[34], the effective mass defined in this way is an average of $\mathbf{m}(i, \mathbf{k})$ around the Fermi level μ, with i the index of the band and $\mathbf{k}$ the wave vector. For electron effective mass, μ was set at the conduction band minimum; for hole effective mass, μ was set at the valence band maximum. Convergence of the effective mass values with respect to the density of k-points over which the band structure was sampled was carefully tested and the values were found to be converged to within 1% using a 20×20×20 mesh.

Chemistries Considered

In this section we provide a brief description of the chemical compositions of the $A_2BB'X_6$ inorganic compounds considered in the present computational studies. We start with 1980 double perovksite compounds with alkali atoms A=Li, Na, K, Rb, Cs, monovalent cations B=Li, Na, K, Rb, Cs, Cu, Ag, Au, Hg, In, Tl, trivalent cations B′=Sc, Y, Al, Ga, In, Tl, As, Sb, Bi and the halide anions X=F, Cl, Br, I. To further motivate the choice of structure and chemistries considered in the calculations, we show in Figure 1(b) a structure map similar to those used in studies of perovskite-based compounds[38]. The axes in this figure correspond to the octahedral factor and the Goldschmidt's tolerance factor.

The octahedral factor is defined as the ratio between average (B,B′) cation Shannon radii for 6-fold coordination and X anion Shannon radius for 6-fold coordination[37]. The tolerance factor is calculated by replacing the B radius in the standard expression for the

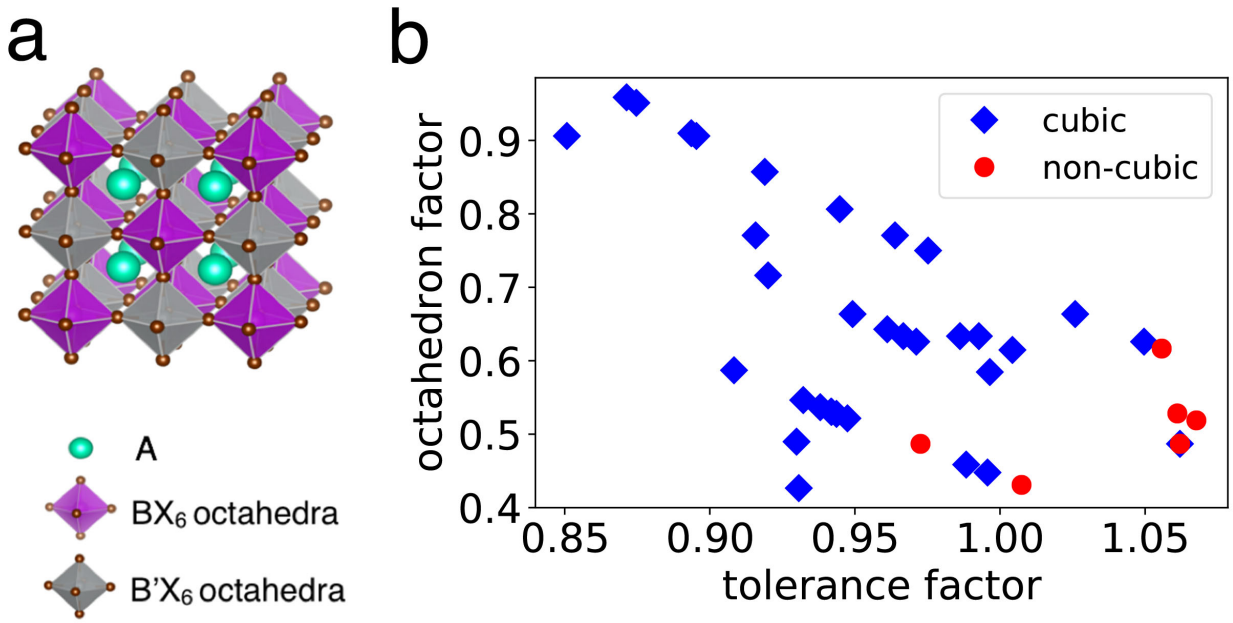

Figure 1: (a) Crystal structure of the cubic double-perovskite compound with composition $A_2BB'X_6$. (b) A structure map for known halide $A_2BB'X_6$ compounds. Crystal structures reported in the ICSD are indicated by the different symbols, with blue diamonds and red circles corresponding to cubic and non-cubic materials, respectively. For each material, the octahedral factor is calculated as $\frac{R_B+R_{B'}}{2R_X}$ and the tolerance factor is calculated as $\frac{R_A+R_X}{\sqrt{2}((R_B+R_{B'})/2+R_X)}$, with R_A, R_B, $R_{B'}$, R_X representing the radii of the A, B and B' site cations and the X site halide anion, respectively. Shannon effective ionic radii for 12-coordinated A^{1+} cations, 6-coordinated B^{1+} and B'^{3+} cations, and 6-coordinated X^{1-} anions[37] are used for R_A, R_B, $R_{B'}$ and R_X.

perovskite tolerance factor[39] with the average radius of (B,B′). For perovskite compounds the octahedral factor is used empirically to predict the formation of the BX_6 octahedron; and the tolerance factor is used empirically to predict the formation and distortion of the perovksite structure. Likewise, in the $A_2BB'X_6$ double perovskite structure, we can combine the octahedral factor and tolerance factor to predict the formation and distortion of the structure.

Small octahedral factors suggest that the formation of BX_6 octahedra are disfavored. According to the survey of known $A_2BB'X_6$ compounds in the ICSD database[40,41], shown in Fig.1(b), most known compounds are face-centered cubic ($Fm\bar{3}m$) and are indicated by blue diamonds. Thus, this work focuses on the consideration of such cubic structures with a $Fm\bar{3}m$ space group. On the other hand, as shown in Fig.1(b), compounds with larger tolerance factor and smaller octahedral factor tend to form non-cubic structures, as indicated by red circle symbols. The crystallographic details of the experimentally observed double perovskite structures are listed in Table S1. The limits of the octahedral factor and tolerance factor for cubic structures indicated by the ICSD survey are used empirically as the first screening criteria to reduce the 1980 compounds by approximately half. The limits for tolerance factor is (0.82, 1.08) and for octahedron factor (0.4, 1.0).

Overview of Database

In Figure 2(a) we presented the distribution of the calculated energy above hull and PBE band gap of all double perovskite halides that are within the determined limits for tolerance factor and octahedral factor identified in the previous section. About half of these 1,149 compounds have energy above hull less than 50meV/atom, which means they are likely to be stable or metastable and synthesizable[42]. It should be pointed out that the Materials Project database does not contain all possible decomposition products for some of the compounds, so that the calculated energy above hull serves only as a lower bound such that the actual thermodynamic (meta)stability could be lower than predicted. This screening step (i.e.,

considering only compounds with energy above hull lower than 50 meV/atom) narrows down the search space for synthesizable double perovksite halides to 569. The calculated PBE band gaps of double perovskite halides span from 0 to 8 eV, which indicates a rich variety of electronic properties, covering metals, semiconductors and large-gap insulators. Out of the 569 compounds, 67, 199, and 303 of them have PBE-calculated band gaps(E_g) of 0, $0 < E_g < 2.5$, $E_g \geq 2.5$, respectively. From the scatter plot in Fig. 2(a) we can observe that compounds with the highest values of the energy above hull (i.e., more unstable) are more likely to be those predicted as metals.

To evaluate the transport properties of these compounds, we perform further calculations of effective masses. In Figure 2(b) we presented the distribution of effective masses and PBE band gaps of 189 double perovskite halides with the energy above hull(E_{hull}) having values < 50 meV/atom and $0.1 < E_g < 2.5$ eV. Interestingly, most of the compounds have very small effective electron masses(167 compounds with $m_e < 1$), but overall a relatively broad hole mass distribution. The groups of outliers are indicated in the scatter plot, and most of them have Sc as B′ site. It is interesting that Sc compounds have such a broad range of effective mass values. For example, Rb_2CuScF_6 has very small electron mass and very large hole mass, while $Rb_2CuScCl_6$ has very large electron mass and an intermediate value of hole mass. The hybridization in Sc-Cl bond and Cu-Cl bond is relatively stronger than Sc-F bond and Cu-F bond, so Cu-d band(valence band) and Sc-d band(conduction band) are narrower in Rb_2CuScF_6 than in $Rb_2CuScCl_6$, thus the effective mass should be larger in Rb_2CuScF_6, which is true for hole mass. However, it happens that in Rb_2CuScF_6 at the conduction band edge there is also some hybridization from Cu-s and F-s, which contributes to a very small electron mass. In $Rb_2CuScCl_6$, the Cu-s and Cl-s also hybridize, but the energy level is higher than the conduction edge, and thus has no contribution to electron effective mass. Other Sc compound outliers in Figure 2(b) generally have large eletron mass due to the narrow Sc-d band that dominates the character of the conduction band edge. Notably, $B/B' = In/Sc$ compounds have small hole masses due to strong In-s/X-p hybridization at valence band,

and might be good for hole transport materials.

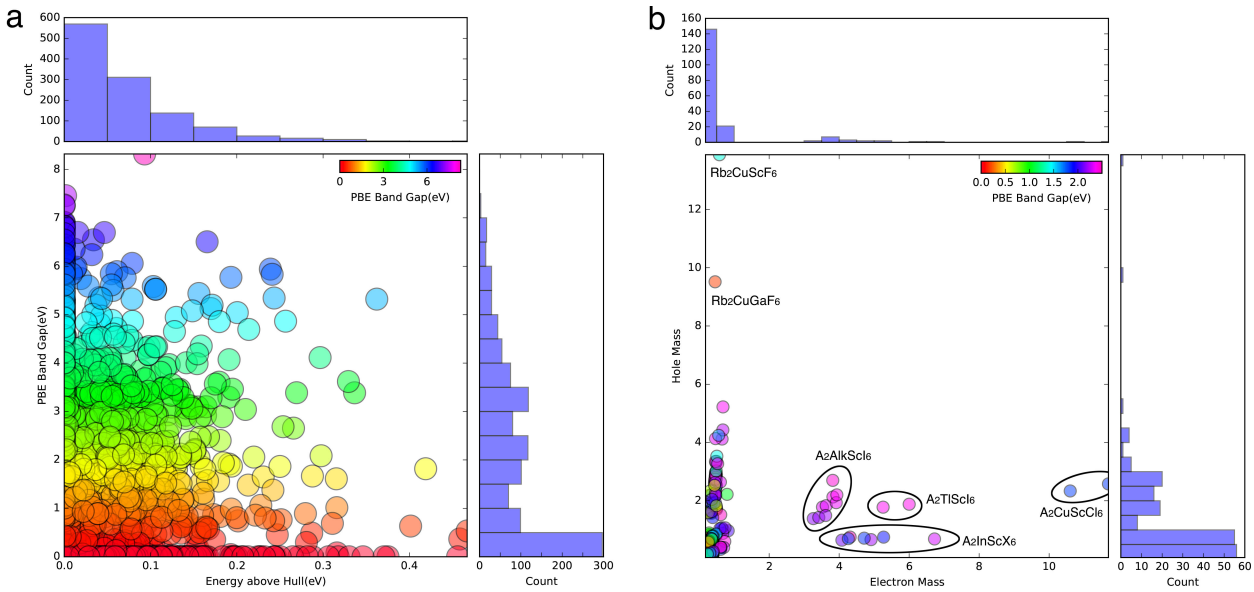

Figure 2: (a) Distribution of calculated energy above hull and PBE band gap. The scatter plot illustrates the distribution of calculated energies above hull and band gap values for 1,149 cubic double perovskite halide compounds. The histograms quantify the distribution of the calculated values for the compounds considered. (b) Distribution of calculated effective mass and PBE band gap values. The scatter plot illustrates the distribution of electron mass and hole mass for 189 double perovskite halides with $E_{hull} < 50$ meV/atom and $0.1 < E_g < 2.5$ eV. The histograms quantify the distribution of the calculated values for the compounds considered.

Analysis for Solar Absorber Applications

Promising Candidates

Among double perovskite halide compounds with $E_{hull} < 50 meV/atom$, only 40 compounds satisfy the following conditions: PBE band gaps with $E_g > 0$ (non-metal), $E_{g(direct)} < 1.5$ eV, and effective masses with $0 < m_e, m_h < 1.5$. Such compounds are considered candidates for potential photovoltaic applications, and are the focus of further analysis. Specifically, for these 40 compounds, we further relax the structure using the HSE functional and calculate band gaps using the HSE functional with SOC included.

We consider first a comparison of the calculated and measured lattice constant of $Cs_2AgBiBr_6$, $Cs_2AgBiCl_6$ and $Cs_2AgInCl_6$. The calculated and measured results agree reasonably well with the GGA-PBE value(11.49 $\mathring{A}$, 10.96 $\mathring{A}$ and 10.68 $\mathring{A}$), which are larger than measurements(11.25 $\mathring{A}$[7], 10.78 $\mathring{A}$[10] and 10.47 $\mathring{A}$[17]) by up to 2.1%. The calculated results from HSE06(10.60 $\mathring{A}$ for $Cs_2AgInCl_6$) show slightly better agreement with measurements, with a deviation of 1.3%. Supplemental Table S2 lists calculated results for the lattice constants of the 40 $A_2BB'X_6$ new compounds that passed all previous screening criteria, and also compares and shows that our GGA-PBE calculated lattice constants are consistent with previous calculations using the same method. For these 40 compounds, except for $Cs_2AgInCl_6$, all other compounds have not been synthesized to our knowledge.

Band gaps, energies above hull and effective masses of the 40 compounds are listed in supplemental Table S3 and Table S4, respectively. The HSE06+SOC calculated band gaps span the range of 0.2 to 2.6 eV. We also list in Table S3 some of the measured band gap and calculated HSE06+SOC band gaps from other work. The calculated HSE06+SOC band gap for $Cs_2AgInCl_6$(2.57 eV) is very close to a previous HSE06 calculation(2.6 eV)[17] without SOC, indicating that SOC effects are not important for In/Ag double perovskites. Both calculations give band gap values somewhat smaller than measurements(3.3 eV)[17]. We can also compare our HSE+SOC calculations with previous calculations for some compounds listed in Table S3. They are mostly consistent with the small differences likely due to the fact that the calculated band gaps are sensitive to the lattice constant and our calculations are based on HSE06 relaxed structures while the previous calculations are based on PBE relaxed structures[23].

The 40 compounds are divided into five categories according to their B and B′ site elements and whether they have direct or indirect band gaps. Similar to halide perovskite ABX_3[43] and derivative A_2BX_6[44] compounds, in the chemical series K, Rb and Cs, the band gap slightly increases(for example, $K_2AgInCl_6$(2.49 eV) to $Rb_2AgInCl_6$(2.52 eV) to $Cs_2AgInCl_6$(2.57 eV)); from Cl to Br to I, the band gap decreases more strongly(for example,

$Rb_2AgInCl_6$(2.52 eV) to $Rb_2AgInBr_6$(1.44 eV) and $Rb_2TlSbBr_6$(1.03 eV) to Rb_2TlSbI_6(0.57 eV)). The chemical trends for B and B′ site elements are more complex and will be discussed further below.

We consider next the results for effective masses listed in Supplemental Table S4. Our calculated average effective masses are consistent with previous calculations, even though previous calculations are based on PBE+SOC band structures and our calculations are based on PBE band structures. The chemical trends in effective mass values listed in Table S4 are correlated with those for the band gaps. Specifically, increasing the size of the A-site cation leads to an increase in both the effective mass and the band gap; increasing the size of the X-site anion leads to a decrease in both the effective mass and the band gap. This correlation between band gap and effective mass is consistent with $k \cdot p$ theory[45]. If we only consider effective mass, among the five categories, the In/Tl-As/Bi/Sb compounds are the best candidates for high mobilities, desirable for photovoltaic applications, since they have small effective mass for both electrons and holes.

In Figure 3 and Figure 4 we present calculated PBE+SOC band structures and densities of states for one representative compound from each of the five categories listed in Table S3, with Figure 3 and Figure 4 showing results for direct and indirect band gap compounds, respectively. Note that the conduction bands are shifted manually to match the HSE+SOC band gaps. We consider first the electronic structure of $Cs_2AgInBr_6$(Figure 3(a)), representative of the set of compounds with B = Cu, Ag, Au and B′ = Al, Ga, In ,Tl. It is calculated to be a direct band gap semiconductor with valence band derived from antibonding states of Ag-d and Br-p orbitals and conduction band derived from antibonding states of In-s and Br-p orbitals. The direct nature of the band gap of $Cs_2AgInBr_6$ is consistent with previous ab initio calculations[25]. The conduction band is very dispersive, leading to its small electron effective mass($0.18m_e$). The valence band edge consists of a heavy hole band and a light hole band, and the average hole effective mass($0.71m_e$) is thus larger than the electron effective mass.

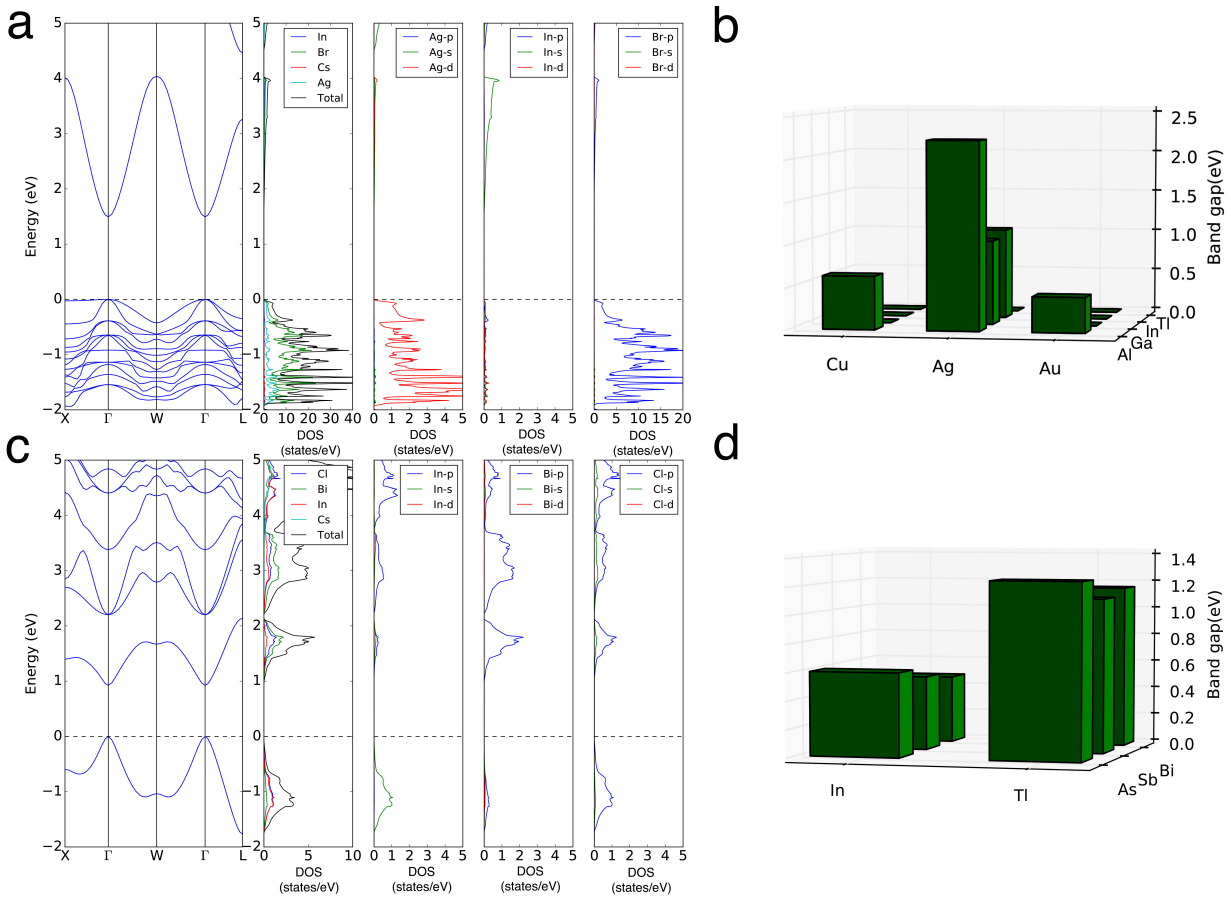

Figure 3: Band structures, total and projected densities of states(DOS), calculated by PBE+SOC with conduction bands shifted to match calculated HSE06+SOC band gaps for (a) $Cs_2AgInBr_6$ and (c) $Cs_2InBiCl_6$. Chemical trends of band gaps calculated by PBE+SOC for $Cs_2BB'Cl_6$ with (c) B = Cu, Ag, Au and B′ = Al, Ga, In ,Tl (d) B = In, Tl and B′ = As, Sb, Bi.

We consider next the representative compound $Cs_2InBiCl_6$ for the set of compounds with B = In, Tl and B′ = As, Sb, Bi. The calculated band structure in Figure 3(c) shows that this compound is a direct band gap semiconductor with valence band derived primarily from antibonding states between In-s and Cl-p orbitals and conduction band primarily from antibonding states between Bi-p and Cl-p orbitals. The direct nature of the band gap of $Cs_2InBiCl_6$ is consistent with previous ab initio calculations[23]. The dispersive nature of both the conduction band and valence band leads to the small electron and hole effective mass($0.39m_e$ and $0.18m_e$).

We consider next the compound Cs_2AgSbI_6 representative of the set of compounds with B = Cu, Ag, Au and B′ = As, Sb, Bi. The calculated band structure in Figure 4(a) shows that this compound is an indirect gap semiconductor with valence band derived from both antibonding states between Ag-d and I-p orbitals and antibonding states between Sb-s and I-p orbitals and conduction band derived from antibonding states between Sb-p and I-p orbitals. The indirect nature of the band gap of Cs_2AgSbI_6 is consistent with previous results reported for similar compounds $Cs_2AgBiBr_6$ and $Cs_2AgBiCl_6$[46]. The conduction band and valence band are both dispersive, leading to small electron and hole effective masses($0.21m_e$ and $0.38m_e$).

Next we consider the compound Cs_2AuScI_6 representative of the set of compounds with B = Cu, Ag, Au and B′ = Sc, Y. The calculated band structure in Figure 4(c) shows that it is an indirect gap semiconductor with valence band derived primarily from antibonding states between Au-d and I-p orbitals and conduction band derived from both antibonding states between Au-s and I-p orbitals and antibonding states between Sc-d and I-p orbitals. To the best of our knowledge, no experimental results have been reported for any of the compounds in this category. The conduction band is more dispersive than the valence band, resulting in a smaller electron effective mass($0.23m_e$) than hole effective mass($0.64m_e$).

We consider finally $Rb_2InInBr_6$, representative of the set of compounds with B and B′ from the same group (Al, Ga, In, Tl) in the periodic table. The calculated band structure

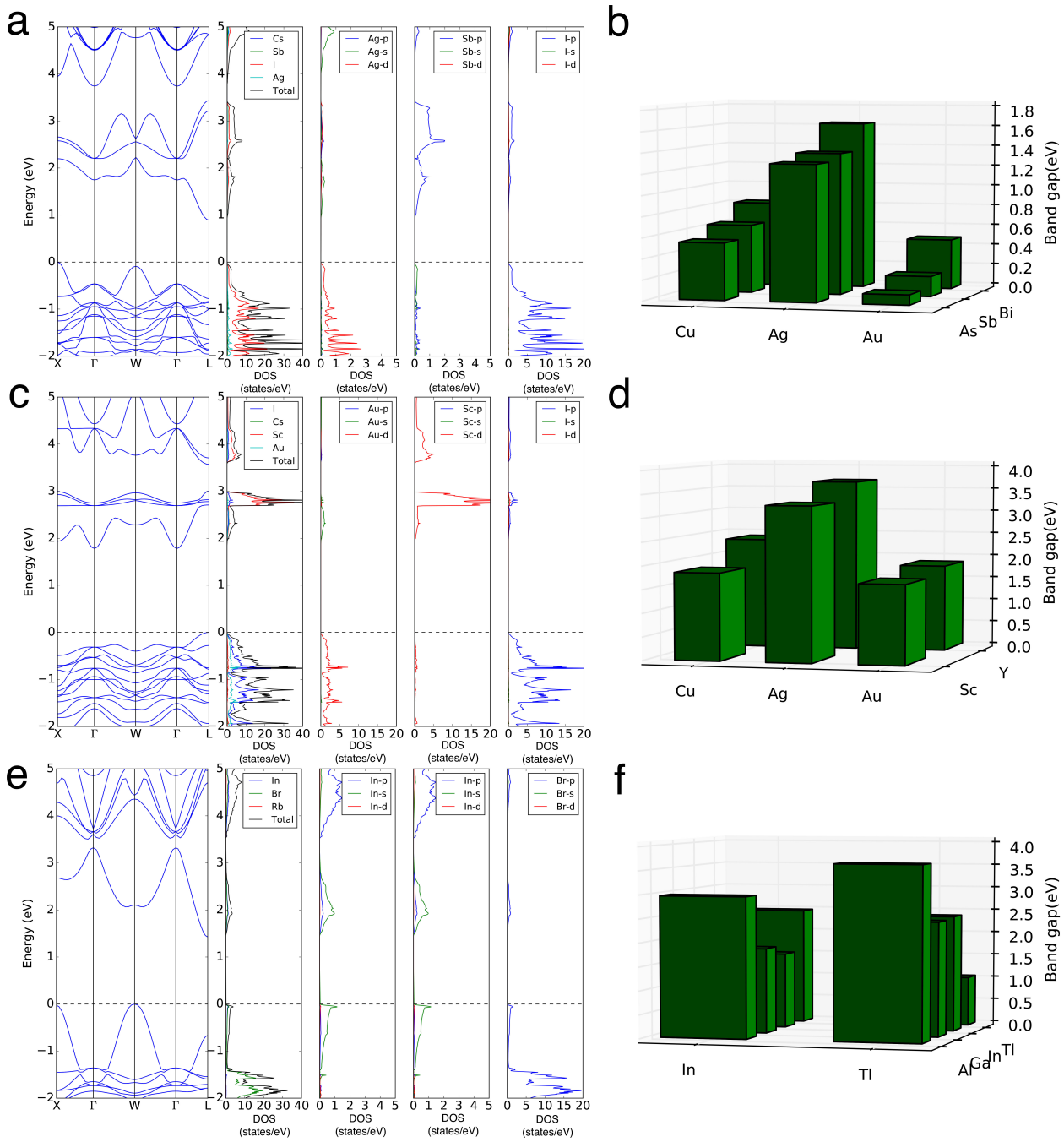

Figure 4: Band structures, total and projected densities of states(DOS), calculated by PBE+SOC with conduction bands shifted to match calculated HSE06+SOC band gaps for (a) Cs_2AgSbI_6, (c) Cs_2AuScI_6 and (e) $Rb_2InInBr_6$. Chemical trends of band gaps calculated by PBE+SOC for $Cs_2BB'Cl_6$ with (b) B = Cu, Ag, Au and B′ = As, Sb, Bi (d) B = Cu, Ag, Au and B′ = Sc, Y and (f) B = In, Tl and B′ = Al, Ga, In, Tl.

in Figure 4(e) shows that it is an indirect band gap semiconductor. If the two In ions in the primitive unit cell are in the same charge state, with one unpaired s electron, we would expect $RbInBr_3$ to be a metallic conductor. Indeed, forcing a single charge state for In by using a 5-atom unit cell results in a metallic state. Charge ordering at the In site leads to the semiconductor state in Figure 4(e), with lower energy than the metallic state. Two similar compounds $CsTlCl_3$ and $CsTlF_3$ have been synthesized and found to be insulators[47]. Labeling the In ion with more charge on it(which we identify as corresponding to the formal 1+ oxidation state) to be In1 and the In ion with less charge on it(which we identify as corresponding to the formal 3+ oxidation state) to be In2, then the valence band of $Rb_2InInBr_6$ is derived from antibonding states between In1-s and Br-p orbitals and conduction band derived from antibonding states between In2-s and Cl-p orbitals. This interpretation is better supported by the crystal orbital Hamilton population analysis in Supplemental Figure S6.

Trends in Band Gaps

Calculated band gap trends obtained with the GGA-PBE functional including SOC effect for $Cs_2BB'Cl_6$ compounds with B = Cu, Ag, Au, In, Tl and B′ = Sc, Y, Al, Ga, In, Tl, As, Sb, Bi are plotted also in Figure 3(b, d) and Figure 4(b, d, f). Again these compounds are divided into 5 categories, with direct band gap ones plotted in Figure 3 and indirect ones in Figure 4. For $Cs_2BB'Cl_6$ compounds with B = Cu, Ag, Au and B′ = Al, Ga, In, Tl(Figure 3(b)), silver compounds have larger band gaps than copper and gold. This is because among Cu, Ag and Au, Ag has the lowest energy d states and the valence band maximum(VBM) derives from hybridization between Cu/Ag/Au-d and Cl-p orbitals, such that the lowest VBM for Ag compounds results in the largest band gap. For $Cs_2AgB'Cl_6$ compounds, the B'=Tl has smaller band gap than B'=In and B'=Ga compounds, which in turn have smaller band gaps than B'=Al compound. This can be understood as resulting from the fact that the cation size decreases from Tl to In to Ga to Al, so that hybridization strength with Cl-p states

increases as a result, leading to increasing conduction band minimum (CBM, antibonding states between Tl/In/Ga-s and Cl-p), thus increasing the band gap value from Tl to In and Ga. For Al compounds, the hybridization is so strong that the antibonding state between Al-s and Cl-p orbitals is too high to be the CBM. The CBM for Al compounds is derived from the antibonding states between Cu/Ag/Au-s and Cl-p orbitals. Cu/Ag/Au-s states are higher than Tl/In/Ga-s states, such that for Al compounds the CBM is still higher than for Tl/In/Ga compounds, so the band gap for the Al compound is the largest.

For $Cs_2BB'Cl_6$ compounds with B = In, Tl and B′ = As, Sb, Bi(Figure 3(d)), Tl compounds have larger band gaps than In compounds. Due to relativistic effects, Tl-s is lower in energy than In-s, resulting in a lower VBM. No consistent trend in band gap was found for the chemical series As, Sb, Bi in these compounds.

For $Cs_2BB'Cl_6$ compounds with B = Cu, Ag, Au and B′ = As, Sb, Bi(Figure 4(b)), silver compounds have the largest band gap among Cu, Ag, and Au compounds, due to the deepest Ag-d states and lowest VBM, as discussed above. For given B site cations, increasing the size of B′ cations increases the band gap. Since the CBM is derived from As/Sb/Bi-p and Cl-p/s hybridization, the increasing p-state energy level going from As to Sb to Bi results in an increasing CBM. This is consistent with reported alloying experiments and first-principle calculations[20].

For $Cs_2BB'Cl_6$ compounds with B = Cu, Ag, Au and B′ = Sc, Y(Figure 4(d)), again silver compounds have the largest band gap among Cu, Ag and Au. For given B site cations, increasing the size of B′ cations(from Sc to Y) increases the band gap. For Cu/Ag compounds, the CBM is mostly derived from Sc/Y-d and Cl-p hybridization, and the d-state energy level increases from Sc to Y, resulting in an increasing CBM. For Au compounds, the CBM is partly derived from Au-s and Cl-p hybridization and partly from Sc/Y-d and Cl-s hybridization, such that the CBM again increases from Sc to Y because of the increased energy of the d level of Y, resulting in an increased band gap from Sc to Y.

For $Cs_2BB'Cl_6$ compounds with B = In, Tl and B′ = Al, Ga, In ,Tl(Figure 4(f), the

chemical trend is more interesting since B and B′ site cations come from the same group. Roughly, the trend is as follows: for the series TlTl, InIn, GaIn, TlGa, TlIn, InAl, TlAl, the band gap value increases from left to right. This trend can be explained by the fact that electronegativity increases from Al to In to Tl to Ga. If we consider $Cs_2TlAlCl_6$ as an example, the CBM is derived from antibonding states between Al-s and Cl-p, and the VBM is derived from antibonding states between Tl-s and Cl-p: the VBM is derived from electronic states associated with the element with larger electronegativity and the CBM is derived from the element with smaller electronegativity. Roughly, the larger difference in electronegativity between the B and B′ elements, the larger band gap we would expect.

Summary

Starting from a consideration of the octahedral and tolerance factors of 2000 candidate double-perovskite compounds, we compute structural, electronic and transport properties of 1000 compounds using first-principles calculations. The computational results have been assembled in a database that is accessible through the Materials Project online. We present the application of the database in screening for new double perovskite halide compounds showing promising electronic properties for photovoltaic solar absorber applications. 40 compounds from 5 categories were identified as promising candidates and chemical trends for band gap within each categories are identified as follows: for all $Cs_2BB'Cl_6$ compounds with B = Cu, Ag, Au and B′=Al, Ga, In, Tl, Sc, Y, As, Sb, Bi, Ag compounds always have larger band gaps than those with Cu and Au with the same B′ elements. For $Cs_2BB'Cl_6$ compounds with B = Cu, Ag, Au and B′ = Al, Ga, In, Tl, the band gap trend for B′ site is Al > In, Ga > Tl. For $Cs_2BB'Cl_6$ compounds with B = In, Tl and B′ = As, Sb, Bi, Tl compounds are found to have larger band gaps than In compounds, confirming results of a previous study[23]. For $Cs_2BB'Cl_6$ compounds with B = Cu, Ag, Au and B′ = As, Sb, Bi, the band gap trend for B′ is Bi > Sb > As. For $Cs_2BB'Cl_6$ compounds with B=Cu, Ag, Au

and B′ = Sc, Y, the band gap increases from Sc to Y. For $Cs_2BB'Cl_6$ compounds with B = In, Tl and B′ = Al, Ga, In, Tl, the larger the difference in electronegativity between B and B′ elements, the larger the calculated band gap. These trends can provide guidelines for the use of substitutional alloying as a means of tuning band structures in halide perovskite solid solutions.

In addition to the potential solar-cell applications discussed specifically in this work, the halide double-perovskite database developed in this work can be used for other applications such as scintillators. For scintillator applications, it is usually required that the host materials have large enough band gap to accommodate dopant-ion energy levels involved in relevant electronic transitions. An overview of our database shows that the compounds with alkali metals as B site cations usually have significantly larger band gaps than compounds with other B site elements. Such compounds can be engineered towards scintillator applications, and indeed the compounds Cs_2LiYCl_6 and $Cs_2NaYBr_3I_3$ have already been identified as relevant examples[4,48]. During our calculations for this database, we also rediscovered and predicted the phenomenon of charge order in $ATlX_3$[47] and $AInX_3$ compounds, respectively. It is possible that some of them may be precursors for superconducting compounds, as discussed in Ref. 47. Overall, it is anticipated that the database of halide double-perovskite compounds developed in this work and made available online could find application in materials discovery efforts for a wide range of applications.

Acknowledgement

This work was funded primarily by the National Research Foundation (NRF), Singapore (CRP NRF2014NRF-CRP002-036 and NRF-CRP14-2014-03) and the Singapore-Berkeley Research Initiative for Sustainable Energy (SinBeRISE) CREATE programme. Use was made of computational resources provided under the Extreme Science and Engineering Discovery Environment (XSEDE), which is supported by the National Science Foundation grant

No. OCI-1053575. The efforts of P.H., K.P. and M.A., associated with the integration of the database into Materials Project (P.H. and K.P.) and supervising the computational work and its analysis (M.A.) was funded by the U.S. Department of Energy, Office of Science, Office of Basic Energy Sciences, Materials Sciences and Engineering Division under Contract No. DE-AC02-05-CH11231 (Materials Project program KC23MP).

References

(1) Greul, E.; Petrus, M. L.; Binek, A.; Docampo, P.; Bein, T. Highly Stable, Phase Pure $Cs_2AgBiBr_6$ Double Perovskite Thin Films for Optoelectronic Applications. *J. Mater. Chem. A* **2017**, *5*, 19972–19981.

(2) Luo, J.; Li, S.; Wu, H.; Zhou, Y.; Li, Y.; Liu, J.; Li, J.; Li, K.; Yi, F.; Niu, G.; Tang, J. $Cs_2AgInCl_6$ Double Perovskite Single Crystals: Parity Forbidden Transitions and Their Application For Sensitive and Fast UV Photodetectors. *ACS Photonics* **2018**, *5*, 398–405.

(3) Pan, W. et al. $Cs_2AgBiBr_6$ Single-crystal X-ray Detectors with a Low Detection Limit. *Nat. Photonics* **2017**, *11*, 726–732.

(4) Glodo, J.; Hawrami, R.; Shah, K. S. Development of Cs_2LiYCl_6 Scintillator. *J. Cryst. Growth* **2013**, *379*, 73–78.

(5) Jain, A.; Ong, S. P.; Hautier, G.; Chen, W.; Richards, W. D.; Dacek, S.; Cholia, S.; Gunter, D.; Skinner, D.; Ceder, G.; Persson, K. The Materials Project: A Materials Genome Approach to Accelerating Materials Innovation. *APL Mater.* **2013**, *1*, 011002–011012.

(6) Chakraborty, S.; Xie, W.; Mathews, N.; Sherburne, M.; Ahuja, R.; Asta, M.; Mhaisalkar, S. G. Rational Design: A High-Throughput Computational Screening and

Experimental Validation Methodology for Lead-Free and Emergent Hybrid Perovskites. *ACS Energy Lett.* **2017**, *2*, 837–845.

(7) Slavney, A. H.; Hu, T.; Lindenberg, A. M.; Karunadasa, H. I. A Bismuth-Halide Double Perovskite with Long Carrier Recombination Lifetime for Photovoltaic Applications. *J. Am. Chem. Soc.* **2016**, *138*, 2138–2141.

(8) Ning, W.; Wang, F.; Wu, B.; Lu, J.; Yan, Z.; Liu, X.; Tao, Y.; Liu, J.-M.; Huang, W.; Fahlman, M.; Hultman, L.; Sum, T. C.; Gao, F. Long Electron–Hole Diffusion Length in High-Quality Lead-Free Double Perovskite Films. *Adv. Mater.* **2018**, *30*, 1706246.

(9) Wei, F.; Deng, Z.; Sun, S.; Zhang, F.; Evans, D. M.; Kieslich, G.; Tominaka, S.; Carpenter, M. A.; Zhang, J.; Bristowe, P. D.; Cheetham, A. K. Synthesis and Properties of a Lead-Free Hybrid Double Perovskite: $(CH_3NH_3)_2AgBiBr_6$. *Chem. Mat.* **2017**, *29*, 1089–1094.

(10) Volonakis, G.; Filip, M. R.; Haghighirad, A. A.; Sakai, N.; Wenger, B.; Snaith, H. J.; Giustino, F. Lead-Free Halide Double Perovskites via Heterovalent Substitution of Noble Metals. *J. Phys. Chem. Lett.* **2016**, *7*, 1254–1259.

(11) McClure, E. T.; Ball, M. R.; Windl, W.; Woodward, P. M. Cs_2AgBiX_6(X = Br, Cl): New Visible Light Absorbing, Lead-Free Halide Perovskite Semiconductors. *Chem. Mater.* **2016**, *28*, 1348–1354.

(12) Creutz, S. E.; Crites, E. N.; De Siena, M. C.; Gamelin, D. R. Colloidal Nanocrystals of Lead-Free Double-Perovskite (Elpasolite) Semiconductors: Synthesis and Anion Exchange To Access New Materials. *Nano Lett.* **2018**, *18*, 1118–1123.

(13) ThaoTran, T.; R.Panella, J.; R.Chamorro, J.; R.Morey, J.; M.McQueen, T. Designing Indirect–direct Bandgap Transitions in Double Perovskites. *Mater. Horizons* **2017**, *4*, 688–693.

(14) Wei, F.; Deng, Z.; Sun, S.; Xie, F.; Kieslich, G.; Evans, D. M.; Carpenter, M. A.; Bristowe, P. D.; Cheetham, A. K. The Synthesis, Structure and Electronic Properties of a Lead-free Hybrid Inorganic–organic Double Perovskite $(MA)_2KBiCl_6$ (MA = Methylammonium). *Mater. Horiz.* **2016**, *3*, 328–332.

(15) Savory, C. N.; Walsh, A.; Scanlon, D. O. Can Pb-Free Halide Double Perovskites Support High-Efficiency Solar Cells? *ACS Energy Lett.* **2016**, *1*, 949–955.

(16) Deng, Z.; Wei, F.; Sun, S.; Kieslich, G.; K.Cheetham, A.; D.Bristowe, P. Exploring the Properties of Lead-free Hybrid Double Perovskites Using a Combined Computational-experimental Approach. *J. Mater. Chem. A* **2016**, *4*, 12025–12029.

(17) Volonakis, G.; Haghighirad, A. A.; Milot, R. L.; Sio, W. H.; Filip, M. R.; Wenger, B.; Johnston, M. B.; Herz, L. M.; Snaith, H. J.; Giustino, F. $Cs_2InAgCl_6$: A New Lead-Free Halide Double Perovskite with Direct Band Gap. *J. Phys. Chem. Lett.* **2017**, *8*, 772–778.

(18) Zhou, J.; Xia, Z.; S.Molokeev, M.; Zhang, X.; Peng, D.; Liu, Q. Composition design, optical gap and stability investigations of lead-free halide double perovskite $Cs_2AgInCl_6$. *J. Mater. Chem. A* **2017**, *5*, 15031–15037.

(19) Slavney, A. H.; Leppert, L.; Bartesaghi, D.; Gold-Parker, A.; Toney, M. F.; Savenije, T. J.; Neaton, J. B.; Karunadasa, H. I. Defect-Induced Band-Edge Reconstruction of a Bismuth-Halide Double Perovskite for Visible-Light Absorption. *J. Am. Chem. Soc.* **2017**, *139*, 5015–5018.

(20) Du, K.-z.; Meng, W.; Wang, X.; Yan, Y.; Mitzi, D. B. Bandgap Engineering of Lead-Free Double Perovskite $Cs_2AgBiBr_6$ through Trivalent Metal Alloying. *Angew. Chem. Int. Ed.* **2017**, *56*, 8158–8162.

(21) Filip, M. R.; Liu, X.; Miglio, A.; Hautier, G.; Giustino, F. Phase Diagrams and Stability

of Lead-Free Halide Double Perovskites $Cs_2BB'X_6$: B = Sb and Bi, B′ = Cu, Ag, and Au, and X = Cl, Br, and I. *J. Phys. Chem. C* **2018**, *122*, 158–170.

(22) Volonakis, G.; Haghighirad, A. A.; Snaith, H. J.; Giustino, F. Route to Stable Lead-Free Double Perovskites with the Electronic Structure of $CH_3NH_3PbI_3$: A Case for Mixed-Cation $[Cs/CH_3NH_3/CH(NH_2)_2]_2InBiBr_6$. *J. Phys. Chem. Lett.* **2017**, *8*, 3917–3924.

(23) Zhao, X.-G.; Yang, J.-H.; Fu, Y.; Yang, D.; Xu, Q.; Yu, L.; Wei, S.-H.; Zhang, L. Design of Lead-Free Inorganic Halide Perovskites for Solar Cells via Cation-Transmutation. *J. Am. Chem. Soc.* **2017**, *139*, 2630–2638.

(24) Meng, W.; Wang, X.; Xiao, Z.; Wang, J.; Mitzi, D. B.; Yan, Y. Parity-Forbidden Transitions and Their Impact on the Optical Absorption Properties of Lead-Free Metal Halide Perovskites and Double Perovskites. *J. Phys. Chem. Lett.* **2017**, *8*, 2999–3007.

(25) Zhao, X.-G.; Yang, D.; Sun, Y.; Li, T.; Zhang, L.; Yu, L.; Zunger, A. Cu–In Halide Perovskite Solar Absorbers. *J. Am. Chem. Soc.* **2017**, *139*, 6718–6725.

(26) Dai, J.; Ma, L.; Ju, M.; Huang, J.; ChengZeng, X. In- and Ga-based Inorganic Double Perovskites with Direct Bandgaps for Photovoltaic Applications. *Phys. Chem. Chem. Phys.* **2017**, *19*, 21691–21695.

(27) Jain, A.; Voznyy, O.; Sargent, E. H. High-Throughput Screening of Lead-Free Perovskite-like Materials for Optoelectronic Applications. *J. Phys. Chem. C* **2017**, *121*, 7183–7187.

(28) Debbichi, L.; Lee, S.; Cho, H.; Rappe, A. M.; Hong, K.-H.; Jang, M. S.; Kim, H. Mixed Valence Perovskite $Cs_2Au_2I_6$: A Potential Material for Thin-Film Pb-Free Photovoltaic Cells with Ultrahigh Efficiency. *Adv. Mater.* **2018**, *30*, 1707001.

(29) Perdew, J. P.; Burke, K.; Ernzerhof, M. Generalized Gradient Approximation Made Simple. *Phys. Rev. Lett.* **1996**, *77*, 3865–3868.

(30) Blöchl, P. E. Projector Augmented-wave Method. *Phys. Rev. B* **1994**, *50*, 17953–17979.

(31) Kresse, G.; Furthmüller, J. Efficient Iterative Schemes for *ab initio* Total-energy Calculations Using a Plane-wave Basis Set. *Phys. Rev. B* **1996**, *54*, 11169–11186.

(32) Kresse, G.; Furthmüller, J. Efficiency of Ab-initio Total Energy Calculations for Metals and Semiconductors Using a Plane-wave Basis Set. *Computational Mater. Sci.* **1996**, *6*, 15–50.

(33) Kresse, G.; Hafner, J. *Ab initio* Molecular Dynamics for Liquid Metals. *Phys. Rev. B* **1993**, *47*, 558–561.

(34) Hautier, G.; Miglio, A.; Ceder, G.; Rignanese, G.-M.; Gonze, X. Identification and Design Principles of Low Hole Effective Mass p-type Transparent Conducting Oxides. *Nat. Commun.* **2013**, *4*, 2292–2298.

(35) Madsen, G. K. H.; Singh, D. J. BoltzTraP. A Code for Calculating Band-structure Dependent Quantities. *Comput. Phys. Commun.* **2006**, *175*, 67–71.

(36) Ong, S. P.; Richards, W. D.; Jain, A.; Hautier, G.; Kocher, M.; Cholia, S.; Gunter, D.; Chevrier, V. L.; Persson, K. A.; Ceder, G. Python Materials Genomics (pymatgen): A Robust, Open-source Python Library for Materials Analysis. *Computational Mater. Sci.* **2013**, *68*, 314–319.

(37) Shannon, R. D. Revised Effective Ionic Radii and Systematic Studies of Interatomic Distances in Halides and Chalcogenides. *Acta Crystallogr. A* **1976**, *32*, 751–767.

(38) Li, W.; Ionescu, E.; Riedel, R.; Gurlo, A. Can We Predict the Formability of Perovskite Oxynitrides from Tolerance and Octahedral Factors? *J. Mater. Chem.A* **2013**, *1*, 12239–12245.

(39) Goldschmidt, V. M. Die Gesetze der Krystallochemie. *Naturwissenschaften* **1926**, *14*, 477–485.

(40) Belsky, A.; Hellenbrandt, M.; Karen, V. L.; Luksch, P. New Developments in the Inorganic Crystal Structure Database (ICSD): Accessibility in Support of Materials Research and Design. *Acta Crystallogr., Sect. B: Struct. Sci* **2002**, *58*, 364–369.

(41) Bergerhoff, G.; Hundt, R.; Sievers, R.; Brown, I. D. The Inorganic Crystal Structure Data Base. *J. Chem. Inf. Comput. Sci.* **1983**, *23*, 66–69.

(42) Sun, W.; Dacek, S. T.; Ong, S. P.; Hautier, G.; Jain, A.; Richards, W. D.; Gamst, A. C.; Persson, K. A.; Ceder, G. The Thermodynamic Scale of Inorganic Crystalline Metastability. *Sci. Adv.* **2016**, *2*, e1600225.

(43) Krishnamoorthy, T.; Ding, H.; Yan, C.; Leong, W. L.; Baikie, T.; Zhang, Z.; Sherburne, M.; Li, S.; Asta, M.; Mathews, N.; Mhaisalkar, S. G. Lead-free Germanium Iodide Perovskite Materials for Photovoltaic Applications. *J. Mater. Chem.A* **2015**, *3*, 23829–23832.

(44) Cai, Y.; Xie, W.; Ding, H.; Chen, Y.; Thirumal, K.; Wong, L. H.; Mathews, N.; Mhaisalkar, S. G.; Sherburne, M.; Asta, M. Computational Study of Halide Perovskite-Derived A_2BX_6 Inorganic Compounds: Chemical Trends in Electronic Structure and Structural Stability. *Chem. Mater.* **2017**, *29*, 7740–7749.

(45) Yu, P. Y.; Cardona, M. *Fundamentals of Semiconductors*, 4th ed.; Springer-Verlag Berlin Heidelberg, 2010.

(46) Filip, M. R.; Hillman, S.; Haghighirad, A. A.; Snaith, H. J.; Giustino, F. Band Gaps of the Lead-Free Halide Double Perovskites $Cs_2BiAgCl_6$ and $Cs_2BiAgBr_6$ from Theory and Experiment. *J. Phys. Chem. Lett.* **2016**, *7*, 2579–2585.

(47) Retuerto, M. et al. Synthesis and Properties of Charge-Ordered Thallium Halide Perovskites, $CsTl^{+}_{0.5}Tl^{3+}_{0.5}X_3$ (X = F or Cl): Theoretical Precursors for Superconductivity? *Chem. Mater.* **2013**, *25*, 4071–4079.

(48) Wei, H.; Du, M.-H.; Stand, L.; Zhao, Z.; Shi, H.; Zhuravleva, M.; Melcher, C. L. Scintillation Properties and Electronic Structures of the Intrinsic and Extrinsic Mixed Elpasolites $Cs_2NaRBr_3I_3$ (R = La, Y). *Phys. Rev. Applied* **2016**, *5*, 024008.